

- Supplementary Material -

Electrical read-out of individual nuclear spin trajectories in a single-molecule magnet spin-transistor

S. Thiele¹, R. Vincent¹, M. Holzmann², S. Klyatskaya³, M. Ruben^{3,4}, F. Balestro¹ and W. Wernsdorfer¹

¹*Institut Néel, CNRS and Université Joseph Fourier, B.P. 166, 38042 Grenoble Cedex 09, France.*

²*LPMMC, Maison de Magistère, Grenoble, and LPTMC, Jussieu, Paris, France*

³*Institute of Nanotechnology (INT), Karlsruhe Institute of Technology (KIT), 76344 Eggenstein-Leopoldshafen, Germany*

⁴*Institut de Physique et Chimie des Matériaux de Strasbourg (IPCMS),*

CNRS-Université de Strasbourg, 67034 Strasbourg, France.

(Dated: June 13, 2013)

CONTENTS

S1. Device fabrication and methods	1
S2. Terbium Double-Decker	1
S3. Nuclear Spin Read-Out	2
S4. Quantum Tunnelling of Magnetization	3
S5. Quantum Monte Carlo Algorithm	3
S6. Dynamical Equilibrium	5
S7. Selection Rules	6
References	6

S2. TERBIUM DOUBLE-DECKER

We used a Terbium (III) bis-phthalocyanine single molecule magnet (SMM), which is a metal-organic complex often called TbPc₂. Its magnetism originates from the eight 4f electrons of the Tb³⁺ ion, which is situated in the coordination center of the complex. The 4f shell is filled according to the Hund's rules, yielding a total orbital momentum of $L = 3$ and a total spin of $S = 3$. Due to a large spin-orbit interaction (≈ 3000 K) the spin and orbital motion are strongly coupled, leading to the total angular momentum quantum number J . According to the third Hund's rule, the new ground-state of the system is given by $J = L + S = 6$. Inside the complex the terbium ion is 8-fold coordinate to the nitrogen atoms of the two phthalocyanine ligands, which are stacked below and above the Tb ion. They are not only encapsulating the terbium and thus preserving its magnetic properties but also enhancing them by means of a ligand field. The Hamiltonian describing this ligand field interaction was found to be [1]:

S1. DEVICE FABRICATION AND METHODS

The non-migrated junctions, consisting of a gold nanowire on an Au/HfO₂ gate, were prepared by cleaning them with acetone, ethanol, isopropanol and oxygen plasma. To transfer the molecules onto the junctions, we dissolved 0.3 mg of a crystalized TbPc₂ molecules in 0.1 mol of dichloromethane, drop casted the solution on the chip, and blow-dried it with N₂. The sample was then mounted on the mixing chamber of a dilution refrigerator, equipped with high-frequency attenuators (thermo-coax microwave filter and π -filters). The molecule-coated nanowire was then broken by electromigration at 4 K, using a voltage ramp with a fast feed back loop in order to stop the current after the opening of the junction. Electric transport measurements were taken using a lock-in amplifier with excitation voltages of 300V. During the presented measurements, the dilution refrigerator had an electronic temperature of about 0.15 K. The refrigerator was equipped with a home-made three-dimensional vector magnet, allowing magnetic field sweeps in three dimensions at field sweep rates up to 0.2 T/s.

$$\mathbf{H}_{\text{LF}} = A_2^0 \langle r^2 \rangle u_2 \mathbf{O}_2^0 + A_4^0 \langle r^4 \rangle u_4 \mathbf{O}_4^0 + A_4^4 \langle r^4 \rangle u_4 \mathbf{O}_4^4 + A_6^0 \langle r^6 \rangle u_6 \mathbf{O}_6^0. \quad (1)$$

The matrices \mathbf{O}_k^q are the so called Stevens operators and are tabulated in [2]. The ligand field parameters $A_k^q \langle r^k \rangle$ are shown in Tab. S1 and were taken from [1]. The coefficients u_k were tabulated by Stevens [3] as $u_2 = -1/99$, $u_4 = 2/16335$ and $u_6 = -1/891891$

$A_2^0 \langle r^2 \rangle$	$A_4^0 \langle r^4 \rangle$	$A_4^4 \langle r^4 \rangle$	$A_6^0 \langle r^6 \rangle$
595.7K	-328.1K	14.4K	47.5K

TABLE S1. Ligand Field parameters of TbPc₂

Additionally an external magnetic field can be applied to the single-molecule magnet. The effect on the energy levels is described by the Zeeman Hamiltonian \mathbf{H}_Z :

$$\mathbf{H}_Z = g_J \mu_B \mathbf{J} \cdot \mathbf{B}, \quad (2)$$

The Zeeman diagram obtained by diagonalizing $\mathbf{H}_{\text{LF}} + \mathbf{H}_{\text{Z}}$ for different magnetic fields is shown in Fig. S1(a). The ground state doublet $m_J = \pm 6$ is separated from the first excited state $m_J = \pm 5$ by several hundreds of Kelvin, leading to an Ising type spin system at low temperatures. Furthermore the term $A_4^4 \langle r^4 \rangle u_4 \mathbf{O}_4^4$ in \mathbf{H}_{LF} is mixing the $m_J = +6$ and $m_J = -6$ state in third order of perturbation, resulting in an anti-crossing in the μK range (see Fig. S1(b)) and thus giving rise to quantum tunneling of magnetization.

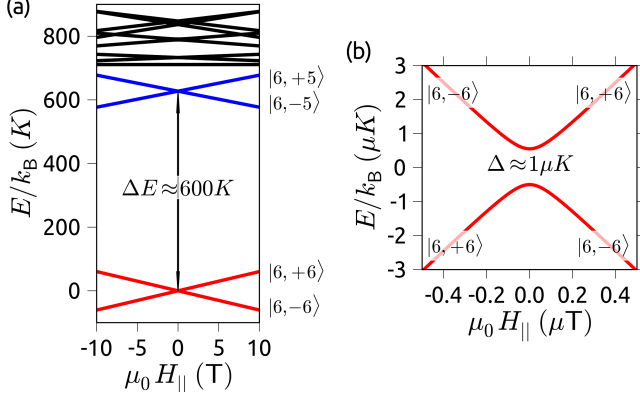


FIG. S1. (a) Zeeman diagram for the TbPc₂. The ground state doublet is separated by 600 K from the first excited state. (b) Zoom on the ground state doublet. Off-diagonal terms in the ligand field Hamiltonian give rise to an avoided level crossing with a Δ of $\approx 1\mu\text{K}$

In addition the hyperfine interaction, coupling the electronic spin \mathbf{J} with the nuclear spin \mathbf{I} and the nuclear anisotropy, has to be included. The Hamiltonian \mathbf{H}_{HF} accounting for this interaction is [4]:

$$\mathbf{H}_{\text{HF}} = A\mathbf{I} \cdot \mathbf{J} + P \left(I_z^2 - \frac{1}{3}I(I+1) \right), \quad (3)$$

$$\mathbf{I} \cdot \mathbf{J} = I_z J_z + \frac{1}{2}(I_+ J_- + I_- J_+), \quad (4)$$

with $A = 24.9$ mK being the hyperfine coupling constant and $P = 14.4$ mK being the quadrupole interaction constant arising from non-perfectly spherical shape of the nucleus. The exact numerical diagonalization of the full Hamiltonian $\mathbf{H} = \mathbf{H}_{\text{LF}} + \mathbf{H}_{\text{HF}} + \mathbf{H}_{\text{Z}}$ results in Fig. 1b of the article.

S3. NUCLEAR SPIN READ-OUT

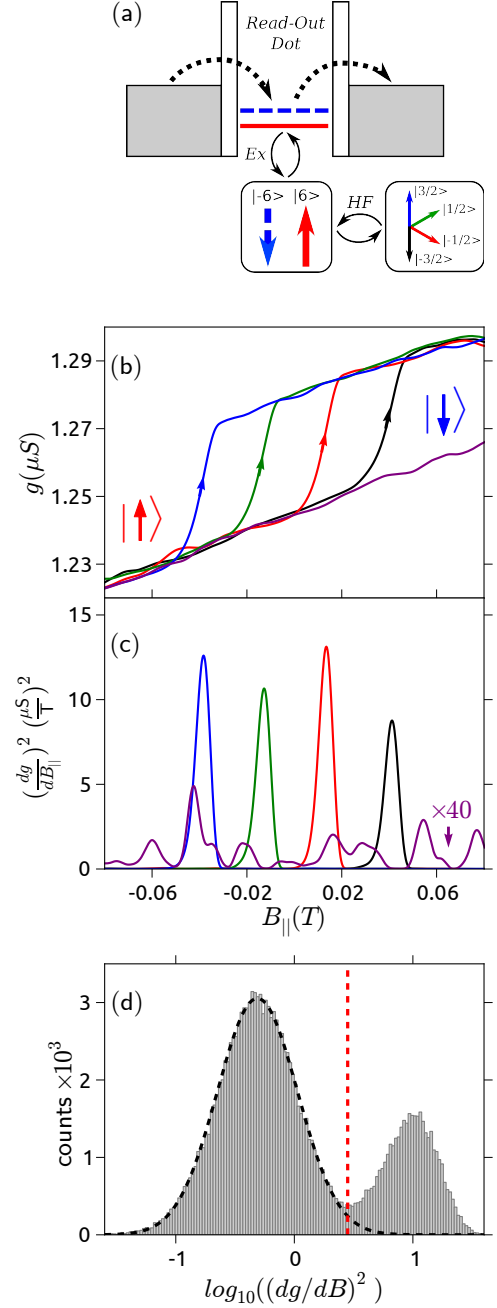


FIG. S2. (a) Simplified model of the single molecule transistor, showing the read-out dot which is electrically coupled to source and drain and the spin dot which is exchange coupled to the read-out dot. The chemical potential of the read-out dot is shifted slightly depending on whether the terbium's electronic spin points up or down. (b) Conductance jumps due to the terbium's electronic spin reversal. The position of the jump depends on the nuclear spin state. (c) Output of the algorithm showing single large peaks at the position of the conductance jumps and many smaller peaks if no jump occurred. (d) Histogram of the amplitude of the signals from (c). Only events on the right of the dotted line are attributed to spin reversals. The events with smaller amplitude are not considered as spin flips and excluded from further treatment.

The single-molecule transistor consists of a source, drain and gated electrodes connected to a read-out dot plus an isolated spin-dot (Tb electronic and nuclear spin) which is exchange coupled to the latter. The electronic transport through the device occurs only inside the read-out dot, leaving the spin-dot protected. However, the exchange coupling which is the link between the two systems is able to slightly change the chemical potential of the read-out dot depending on the orientation of the terbium's electronic spin (Fig. S2(a)). The magnitude of the ferromagnetic coupling was obtained by analyzing the magnetic field behavior of the read-out dot's Kondo-ridge, as presented in Ref. [5]. The lower boundary was estimated to be 200 mT and suggests that the read-out dot is created by the two Pc ligands. As explained in the main article the electronic spin reversal is governed by the quantum tunneling of magnetization (QTM), which happens only at effective zero field. Due to the hyperfine coupling the position of having effective zero magnetic field depends on the orientation of the nuclear spin and thus opens a way to read-out the nuclear spin state.

For the configuration shown in Fig. S2(b) the conductance through the read-out dot is smaller if the terbium's electronic spin is in the $|+6\rangle$ state. Flipping the spin due to a QTM transition changes the conductance by around 3% (Fig. S2(b)). The smear-out effect originates from the finite response time of the lock-in amplifier. What is left to identify the state of the nuclear spin is the determination of the conductance jump position. Due to the large amount of data this is done by an algorithm [6], which calculates in essence the square of the first derivative (Fig. S2(c)) yielding a peak whose maximum indicates the switching field. If no switching occurs the height of the peaks determined by the algorithm is in average more than forty times smaller. Possible spin flips are up-down or down-up resulting in positive or negative peaks after applying the algorithm, respectively. The actual state of the electronic spin prior to the measurement is not determined and therefore both spin reversal are possible. Thus the position and amplitude of the largest positive and negative peak are computed for every measurement.

In order to sort out the spin-flips from measurements with on event the amplitudes of all detected maxima and minima are plotted in a histogram (Fig. S2(d)). Measurements without a spin-flip event yield the Gaussian-like distribution at the left (small peak amplitude) whereas the peaks due to a spin reversal yield the Gaussian-like distribution on the right (large peak amplitudes). The area under the left Gaussian is roughly 3 times larger than the area under the right Gaussian. The explanation comes from the QTM transition, occurring with a probability of 50% in our experiment and from the fact that every measurement yields two peaks (positive and negative) but only one can be a spin-flip. Therefore 25% of all the events plotted in Fig. S2(d) are spin-reversals. To separate them from the rest of the data a threshold (red dotted line) is introduced. Peaks with an amplitude larger than the threshold are considered to be

spin-reversals. The overlap with the left Gaussian in Fig. S2(d) is around 4%. In a second step we check the magnetic field of the remaining events. All jumps occurring outside a window of 6 mT (5%) around the theoretical QTM transition are ambiguous and excluded from further treatment. They appear mainly due to the tail of the left peak in Fig. S2(d). Afterwards the remaining data points are attributed to the corresponding nuclear spin state resulting in the time trajectory (black curve Fig.S3).

S4. QUANTUM TUNNELLING OF MAGNETIZATION

The magnetization reversal of the terbium electron spin around zero magnetic field is governed by the quantum tunneling of magnetization. It is a quantum-mechanical process and arises from a finite overlap between different spin states. The probability of having such a transition is given by the Landau-Zener (LZ) formula [7]:

$$P_{LZ} = 1 - \exp \left[-\frac{\pi \Delta^2}{2\hbar g_J \mu_B \Delta m_J \mu_0 dH_z/dt} \right]. \quad (5)$$

It depends on the energy gap Δ of the avoided level crossing and the magnetic field sweep rate (dH_z/dt). Since there are four anti-crossings, one for each nuclear spin state, we observed four different QTM transitions. To show that the energy gap is nuclear spin independent, we measured the tunnel probabilities for each of the anti-crossing (Fig. S4). We found that for a sweep rate of 50 mT/s the average $P_{LZ} \approx 51\%$. The experimental deviation from this value is very small and within the experimental error.

S5. QUANTUM MONTE CARLO ALGORITHM

The nuclear spin trajectories were obtained under non-thermal equilibrium conditions. In order to separate the dynamical processes caused by sweeping the magnetic field from the relaxation and excitation processes caused by coupling the nuclear spin to a thermal bath, we chose a computational approach. A suited algorithm to handle this problem is the quantum Monte Carlo wave function method [8–10]. It divides the simulation into finite time steps dt and iteratively calculates the stochastic evolution of the atomic wave function and hence the nuclear spin trajectory. To do so we supposed the wave function of the isolated system $|\Psi\rangle$ is entirely described by the Hamiltonian \mathbf{H}_0 and all environmental contributions are combined in a perturbation Hamiltonian \mathbf{H}_1 . To calculate the unnormalized wave function $\tilde{\Psi}$ after a small time step we first apply the usual Schrödinger equation:

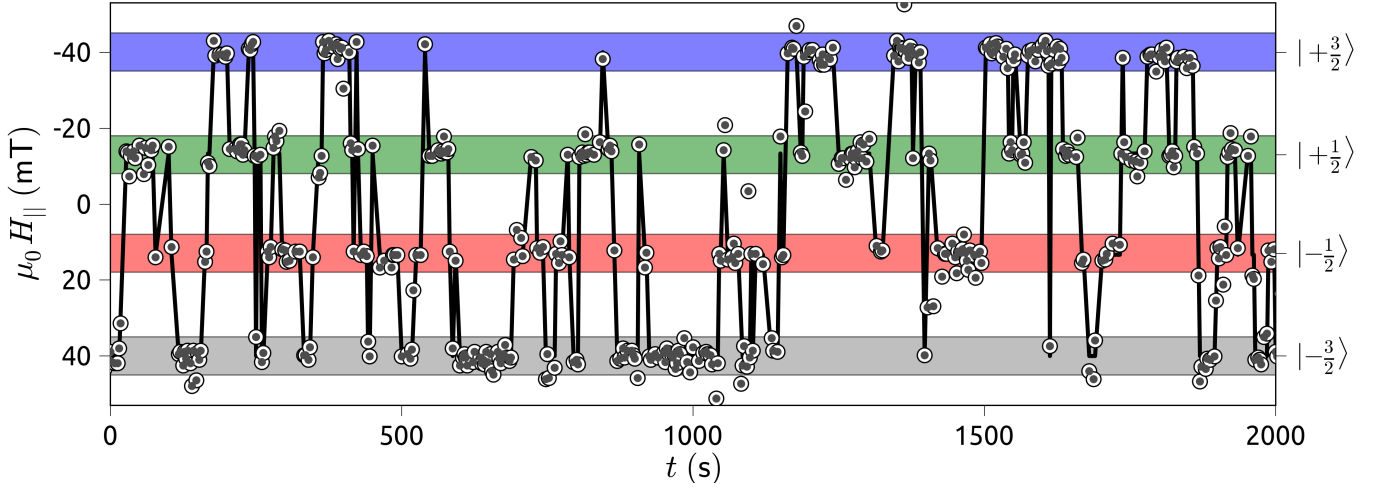


FIG. S3. Trajectory of the nuclear spin (black line) for a time interval of 2000 s. The grey dots are the conductance jump positions and are used to identify the nuclear spin state. If the jump appears within the colored zone it was attributed to the corresponding state otherwise it was considered as noise

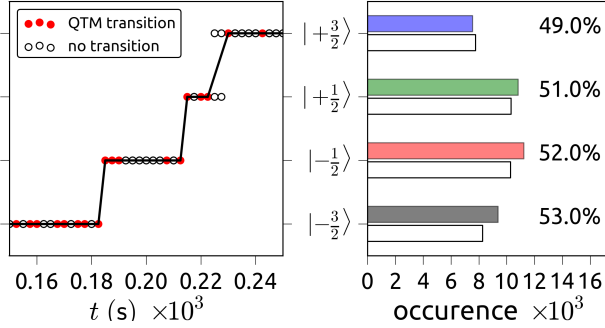


FIG. S4. (a) Nuclear spin trajectory (black line) obtained by different conductance jumps (red dots). Since the tunnelling of the electron spin is a probabilistic event, not every measurement shows a QTM jump (white dots). If we missed a QTM transition, but the nuclear spin did not change between two conductance jumps, we attributed this to the particular spin state. If, however, we missed a tunnel event and the nuclear spin did change, we added a missed event to the state before and after the jump. (b) Histograms of all measured (coloured bars) and missed (white bars) tunnel events for each nuclear spin state, obtaining the individual QTM probabilities.

$$\frac{d\tilde{\Psi}}{dt} = -\frac{i}{\hbar}(\mathbf{H}_0 + \mathbf{H}_1)\Psi. \quad (6)$$

If we assume that \mathbf{H}_1 and \mathbf{H}_0 commute, which is true up to an error of dt^2 we get:

$$\tilde{\Psi}(t + dt) = \exp\left(-\frac{i}{\hbar}\mathbf{H}_1 dt\right) \exp\left(-\frac{i}{\hbar}\mathbf{H}_0 dt\right) \Psi(t). \quad (7)$$

Furthermore we can choose dt in a way that $|\frac{i}{\hbar}\mathbf{H}_1 dt| \ll 1$, then the term $\exp(-\frac{i}{\hbar}\mathbf{H}_1 dt)$ can be written in a first

order Taylor series expansion $\exp(-\frac{i}{\hbar}\mathbf{H}_1 dt) \approx 1 - \frac{i}{\hbar}\mathbf{H}_1 dt$. Since we are only interested in the amplitude of the wave function the term $\exp(-\frac{i}{\hbar}\mathbf{H}_0 dt)$ will be neglected in the following. It adds only a phase term to the wave function and can be reintroduced at any point if necessary. The amplitude of the wave function after a time step dt is therefore:

$$\tilde{\Psi}(t + dt) = \left(1 - \frac{i}{\hbar}\mathbf{H}_1 dt\right) \Psi(t). \quad (8)$$

We can define the Hamiltonian \mathbf{H}_1 as a sum of the relaxation operator \mathbf{C}_1 and the excitation operator \mathbf{C}_2 :

$$\mathbf{H}_1 = -\frac{i\hbar}{2} \sum_m \mathbf{C}_m^\dagger \mathbf{C}_m. \quad (9)$$

By expanding Eqs. 2,3 and writing them in a matrix form we get:

$$\mathbf{C}_1 = \begin{pmatrix} 0 & 0 & 0 & 0 \\ \sqrt{\Gamma_{0,1}(1+n_{0,1})} & 0 & 0 & 0 \\ 0 & \sqrt{\Gamma_{1,2}(1+n_{1,2})} & 0 & 0 \\ 0 & 0 & \sqrt{\Gamma_{2,3}(1+n_{2,3})} & 0 \end{pmatrix},$$

$$\mathbf{C}_2 = \begin{pmatrix} 0 & \sqrt{\Gamma_{0,1} \cdot n_{0,1}} & 0 & 0 \\ 0 & 0 & \sqrt{\Gamma_{1,2} \cdot n_{1,2}} & 0 \\ 0 & 0 & 0 & \sqrt{\Gamma_{2,3} \cdot n_{2,3}} \\ 0 & 0 & 0 & 0 \end{pmatrix}.$$

Note that only transitions with $\Delta m_J = \pm 1$ are considered. The term $n(\omega_{i,j}, T) = [\exp(\hbar\omega_{i,j}/k_B T) - 1]^{-1}$ is the Bose-Einstein distribution function and $\Gamma_{i,j}$ is the transition rate between the i th and the j th nuclear spin state. Since \mathbf{H}_1 has imaginary eigenvalues the wave function $\tilde{\Psi}(t + dt)$ is not normalized. Up to an error of dt^2

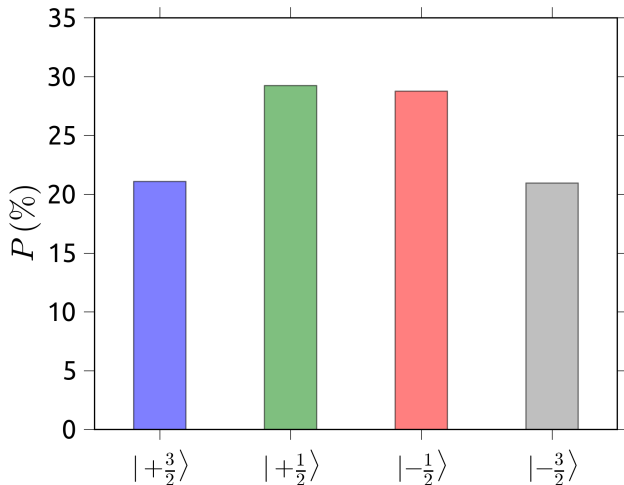


FIG. S5. Simulated time-average occupation probabilities of the four nuclear spin states. The increase in probability for $m_1 = \pm 1/2$ with respect to $m_1 = \pm 3/2$ originates from the asymmetric transition rates $\Gamma_{i,j}$ in combination with periodic repetitions of the measurement. Thus instead of having an equal probability for each nuclear spin state we actively pump the population into $m_1 = \pm 1/2$.

we can write:

$$\langle \Psi(t+dt) | \tilde{\Psi}(t+dt) \rangle = 1 - \delta p, \quad (10)$$

with

$$\delta p = \frac{i}{\hbar} dt \langle \Psi(t) | \left(\mathbf{H}_1 - \mathbf{H}_1^\dagger \right) | \Psi(t) \rangle, \quad (11)$$

being the transition probability per time step dt . Inserting Eq. 9 into Eq. 11 allows for the calculation of the excitation and relaxation probabilities δp_{rel} and δp_{ex} , respectively:

$$\delta p_{\text{rel}} = dt \langle \Psi(t) | \mathbf{C}_1^\dagger \mathbf{C}_1 | \Psi(t) \rangle, \quad (12)$$

$$\delta p_{\text{ex}} = dt \langle \Psi(t) | \mathbf{C}_2^\dagger \mathbf{C}_2 | \Psi(t) \rangle. \quad (13)$$

The non-reversibility of the transition is introduced by a pseudo random variable ϵ . If $\epsilon > \delta p$ the systems stays in the same state and nothing happens. If however $\epsilon < \delta p$ the nuclear spin undergoes a quantum jump and the new wave function is calculated as:

$$\epsilon < \delta p_{\text{rel}} \xrightarrow{\text{relaxation}} \Psi(t+dt) = \frac{\mathbf{C}_1 \tilde{\Psi}(t)}{\sqrt{dt/\delta p}}, \quad (14)$$

$$\epsilon > \delta p_{\text{rel}} \xrightarrow{\text{excitation}} \Psi(t+dt) = \frac{\mathbf{C}_2 \tilde{\Psi}(t)}{\sqrt{dt/\delta p}}. \quad (15)$$

The denominator in Eqs. 14 and 15 accounts for the re-normalization of the wave function. To simulate the sweeping of the magnetic field we group the simulation into intervals of $\Delta t = 2.5$ s. Within each interval we allow

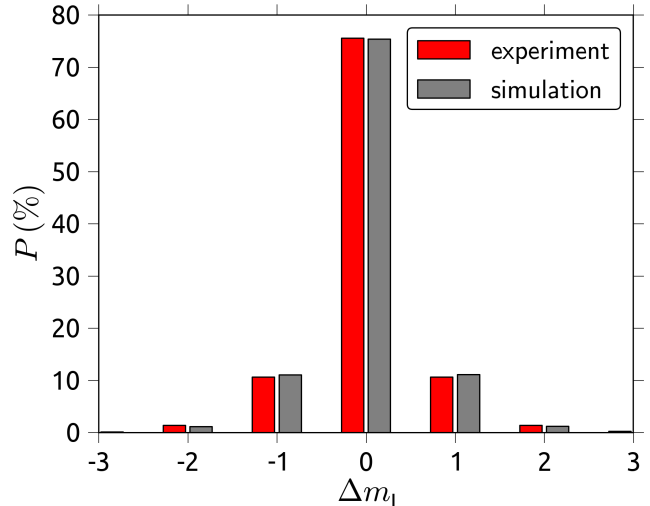


FIG. S6. The experimental distribution (red bars) of Δm_1 is compared with the computed one (grey bars). Since the computer model only allows for transitions with $\Delta m_1 = \pm 1$ we concluded that all higher order transitions are just two or three subsequent transitions with $\Delta m_1 = \pm 1$, which could not be resolved due to finite time sampling Δt .

for the electron spin reversal according to the Landau-Zener probability at four different instants. Therefore we introduced an additional pseudo random number ξ . If we reached the instant corresponding to the current nuclear spin and $\xi < P_{\text{LZ}}$ we inverted all nuclear energy levels. Since the Landau-Zener probability is roughly 0.5 the energy level are inverted every 5 s in average. Within this 5 s the nuclear spin constantly tries to exchange energy with the thermal bath. A several days long nuclear spin trajectory could be calculated within few minutes on a standard PC.

S6. DYNAMICAL EQUILIBRIUM

Every time we reverse the electron spin due to a QTM transition the ground state and the excited states are swapped. Since the swapping period is smaller than T_1 , the time-average population of the nuclear spin converges to a dynamical equilibrium which is far from the Boltzmann distribution. We realized that the probability for $m_1 = \pm 1/2$ is higher than the probability for $m_1 = \pm 3/2$ (see Fig. 3b of the main text). The QMC simulations allowed us to explain this effect. Indeed, the shape of the time-average population in the case where the sweeping period Δt is smaller than T_1 is mainly governed by the individual transition rates $\Gamma_{i,j}$. As shown in Fig.5 of the main article, $\Gamma_{0,1}$ is smaller than $\Gamma_{2,3}$, which means that it is faster to get from the most excited state into the $m_1 = \pm 1/2$ than from the latter into the ground state. Due to this asymmetry and the periodic repetition of the measurement we are actively pumping the popula-

tion into $m_l = \pm 1/2$ states. This result could be nicely reproduced by simulations (see Fig. S5). Notice that for equal $\Gamma_{i,j}$'s the time-average population would be flat, i.e. every state is occupied 25% of the time.

S7. SELECTION RULES

When we recorded the nuclear spin trajectory we observed sometimes transitions with $\Delta m_l \neq \pm 1$. Therefore we were wondering if this effect arises from a finite time resolution, i.e. subsequent $\Delta m_l = \pm 1$ between two subsequent measurements or an additional transition path which allows for $\Delta m_l \neq \pm 1$. To answer this question we compared experimental and simulated data (see Fig. S6). In the latter we took only $\Delta m_l = \pm 1$ transitions into consideration. The perfect agreement supports our assumption that the nuclear spin can only perform quantum jumps which change its quantum number by one.

-
- [1] N. Ishikawa, M. Sugita, T. Okubo, N. Tanaka, T. Iino, and Y. Kaizu, *Inorganic chemistry* **42**, 2440 (2003).
 - [2] A. Abragam and B. Bleaney, *Electron Paramagnetic Resonance of Transition Ions*, p. 944, Oxford Classic Texts in the Physical Sciences, Oxford University Press, US, (2012).
 - [3] K. W. H. Stevens, *Proceedings of the Physical Society, Section A* **65**, 209 (1952).
 - [4] N. Ishikawa, M. Sugita, and W. Wernsdorfer, *Angewandte Chemie (International ed. in English)* **44**, 2931 (2005).
 - [5] R. Vincent, S. Klyatskaya, M. Ruben, W. Wernsdorfer, and F. Balestro, *Nature* **488**, 357 (2012).
 - [6] W. Y. Liu, I. E. Mangin, and G. Gimenez, *Traitement du Signal* **12**, 225 (1995).
 - [7] Wolfgang Wernsdorfer, *International Journal of Nanotechnology* **7**, 497 (2010).
 - [8] J. Dalibard, Y. Castin, and K. Mølmer, *Physical Review Letters* **68**, 580 (1992).
 - [9] K. Molmer, Y. Castin, and J. Dalibard, *Journal of the Optical Society of America B* **10**, 524 (1993).
 - [10] K. Molmer and Y. Castin, *Quantum and Semiclassical Optics: Journal of the European Optical Society Part B* **8**, 49 (1996).